New Nanocomposite Materials Reinforced with Flax Cellulose Nanocrystals in Waterborne Polyurethane

Xiaodong Cao, Hua Dong, and Chang Ming Li*

School of Chemical and Biomedical Engineering, Nanyang Technological University, Singapore 639798, and Center for Advanced Bionanosystems, Nanyang Technological University, Singapore 637457

Received October 30, 2006; Revised Manuscript Received January 10, 2007

New nanocomposite films were prepared from a suspension of cellulose nanocrystals as the filler and a polycaprolactone-based waterborne polyurethane (WPU) as the matrix. The cellulose nanocrystals, prepared by acid hydrolysis of flax fiber, consisted of slender rods with an average length of 327 ± 108 nm and diameter of 21 ± 7 nm, respectively. After the two aqueous suspensions were mixed homogeneously, the nanocomposite films were obtained by casting and evaporating. The morphology, thermal behavior, and mechanical properties of the films were investigated by means of attenuated total reflection Fourier transform infrared spectroscopy, wide-angle X-ray diffraction, differential scanning calorimetry, scanning electron microscopy, and tensile testing. The results indicated that the cellulose nanocrystals could disperse in the WPU uniformly and resulted in an improvement of microphase separation between the soft and hard segments of the WPU matrix. The films showed a significant increase in Young's modulus and tensile strength from 0.51 to 344 MPa and 4.27 to 14.86 MPa, respectively, with increasing filler content from 0 to 30 wt %. Of note is that the Young's modulus increased exponentially with the filler up to a content of 10 wt %. The synergistic interaction between fillers and between the filler and WPU matrix played an important role in reinforcing the nanocomposites. The superior properties of the new nanocomposite materials could have great potential applications.

Introduction

The ability to have different types of molecular architectures specifically designed for each application has made polyurethane (PU) one of the most popular polymers used in a variety of products, such as coatings, adhesives, flexible and rigid foams, elastomers, tough solids, and so forth.[1] However, the conventional polyurethane products usually contain a significant amount of organic solvents and sometimes even free isocynate monomers.[2] Therefore, they have been gradually replaced by the waterborne polyurethanes (WPU) in past decades due to their health and environmental safety.[3−6] As Busato reported, waterborne products, including both architectural and industrial paints, accounted for an estimated 50% of the paint and coatings consumption in Western Europe in 2002 and will represent over 55% of total Europe paint consumption by the year 2010.[7] WPU has many of the features related to conventional organic solvent-borne PU with the advantages of low viscosity at high molecular weight, nontoxicity, and good applicability.[8] The thermal stability, insolubility, and mechanical properties of the WPU, however, are still lower than those of the organic solvent-borne PU and need to be improved.[9] Nanosized particle additives are used as an effective strategy to alter and enhance the properties of WPU. Various types of filler, such as clay,[10−13] multiwalled carbon nanotubes,[14−16] and Au,[17] have been tested, and the results demonstrated a good dispersion of fillers in the WPU matrix and significant improvement of the performances of the nanocomposite materials such as mechanical properties, thermal stability, and others.

More recently, there is an increased use of cellulose nanocrystals (CNs) as the loading-bearing constituent in developing new and inexpensive biodegradable materials due to a high aspect ratio, a high bending strength of about 10 GPa, and a high Young's modulus of approximately 150 GPa.[18,19] As compared to other inorganic reinforcing fillers, CNs have many additional advantages, including a positive ecological, wide variety of fillers available throughout the world, low density, low-energy consumption in manufacturing, ease for recycling by combustion, high sound attenuation, and comparatively easy processability due to their nonabrasive nature, which allows high filling levels, in turn resulting in significant cost savings.[20,21] Since the first announcement of using cellulose nanocrystals from tunicin (an animal cellulose) as a reinforcing phase in a matrix of latex by Favier et al.,[22] the use of CNs from various sources such as cotton,[23] tunicate,[24,25] algae,[26,27] bacteria,[28,29] ramie,[30] and wood[31,32] for the preparation of high performance composite materials has been investigated extensively. Both natural and synthetic polymers were explored as the matrixes. Natural polymers such as poly (β-hydroxyoctanoate) (PHO),[33−35] starch,[36,37] silk fibroin,[38] and cellulose acetate butyrate (CAB)[30] reinforced with cellulose whiskers were reported. Poly-(styrene-*co*-butyl acrylate) (poly(S-*co*-BuA)),[24−39] poly(vinyl chloride) (PVC),[40] polypropylene,[41] waterborne epoxy,[42,43] and poly-(oxyethylene)[44] were used as synthetic matrixes. To our knowledge, however, research on CNs as fillers for reinforcing of WPU can hardly be found in the literature.

The flax plant (Linum usitatissimum) is a member of the Linaceae family, which is an important crop in many regions of the world. Fibers from flax have been used for thousands of years to make different textile products because of their excellent fiber characteristics.[45] Therefore, the search on short fibers from flax as a replacement for synthetic fibers in many non-textile products, for example, in polymer compounds, building materials, textiles, and absorbent materials, has attracted much attention in the past decade.[46] In the present work, we attempt to prepare CNs from flax fiber by acid hydrolysis of concentrated sulfuric

* To whom correspondence should be addressed. Phone: 65-6790-4485. Fax: 65-6790-4485. E-mail: ecmli@ntu.edu.sg.

10.1021/bm0610368 CCC: $37.00
Published on Web 02/22/2007

acid and then use the resulting CNs to reinforce polycaprolactone (PCL)-based WPU for the preparation of a nanocomposite material with improved performances. The resulting materials were prepared by casting the mixture of aqueous suspensions of CNs and WPU in various weight ratios. The morphology, structure, and performance of the resulting nanocomposite films were investigated by attenuated total reflections Fourier transform infrared spectroscopy (ATR-FTIR), scanning electron microscopy (SEM), wide-angle X-ray diffraction (WAXD), differential scanning calorimetry (DSC), and measurement of the mechanical properties.

Experimental Section

Materials. Raw flax fiber was supplied by Biolin Research Inc., Canada. Polycaprolactone diol (M_n = 1250), isophorone diisocyanate (IPDI), dimethylol propionic acid (DMPA), triethylamine (TEA), acetone, sodium hypochlorite solution (available chlorine 10−13%), and concentrated sulfuric acid (98%) were purchased from Sigma-Aldrich Corp. and used as received without further purification.

Preparation of FCNs. A colloidal suspension of cellulose nanocrystals in water was prepared by acid-catalyzed hydrolysis of flax fiber as described by Dong et al.[47] Briefly, the flax fiber (30 g) was first cut into small fragments and mixed with sulfuric acid aqueous solution (250 mL, 64%) and stirred vigorously at 45 °C for 4 h. Subsequently, the suspension was neutralized with sodium hydroxide aqueous solution (40%), discolored by sodium hypochlorite solution, and washed by dialyzing. The dispersion of flax cellulose nanocrystals (FCNs) with a solid content of 1.4 wt % was obtained through 30 min ultrasonic treatment. The suspension did not sediment or flocculate as a consequence of surface sulfate groups created during the sulfuric treatment.[47,48]

Synthesis of WPU. Polycaprolactone diol (60 g) and DMPA (4.02 g) were introduced into a four-necked flask equipped with a mechanical stirrer, condenser, and thermometer, and the mixture was heated to 85 °C until the polycaprolactone diol was melted completely; then IPDI (24.6 g) was added dropwise, and the reaction was carried out in dry nitrogen atmosphere for 4 h. Subsequently, about 80 mL of acetone was poured into the flask to reduce the viscosity of prepolymer and then cooled to 60 °C. After neutralization of carboxylic groups of DMPA with TEA (3.01 g) for 30 min, the product was dispersed with distilled water under vigorous stirring. After the mixture was stirred at room temperature overnight, the acetone was removed by rotary vacuum evaporating at 30 °C, and the solid content of the WPU was 28 wt % finally.

Preparation of the WPU/FCNs Nanocomposite Films. To obtain final dry composite films with 0−30 wt % of solid FCNs in WPU matrix, the suspensions of FCNs and WPU were mixed with various proportions. After mixing, the resulting mixtures were stirred on a rotavapor under vacuum for 15 min to remove the remaining air and thereby avoid the formation of irreversible bubbles during the water evaporation process. Next, they were cast in polystyrene square Petri dishes and dried in a ventilated oven at 50 °C for 10−20 h (depending on the water content). By changing the contents of FCNs over the range of 0, 5, 10, 15, 20, 25, and 30 wt %, a series of nanocomposite films with a thickness of around 0.3 mm were prepared and coded as WPU, WPU/FCNs-5, WPU/FCNs-10, WPU/FCNs-15, WPU/FCNs-20, WPU/FCNs-25, and WPU/FCNs-30, respectively. Before various characterizations, the resulting films were conditioned at room temperature in a desiccator containing P_2O_5 with 0% relative humidity (RH).

Characterizations. ATR-FTIR spectroscopy was performed on a Nicolet ATR-FTIR spectrometer outfitted with a germanium crystal (AVATAR 360, U.S.) at room temperature and fixed angle of incidence (45°). The samples with thickness of about 0.3 mm were taken at random from sheets and placed flat on the crystal surface. The data were collected over 16 scans with a resolution of 4 cm^{-1}. The background spectra were recorded with Ge crystal contacting air in the absence of samples.

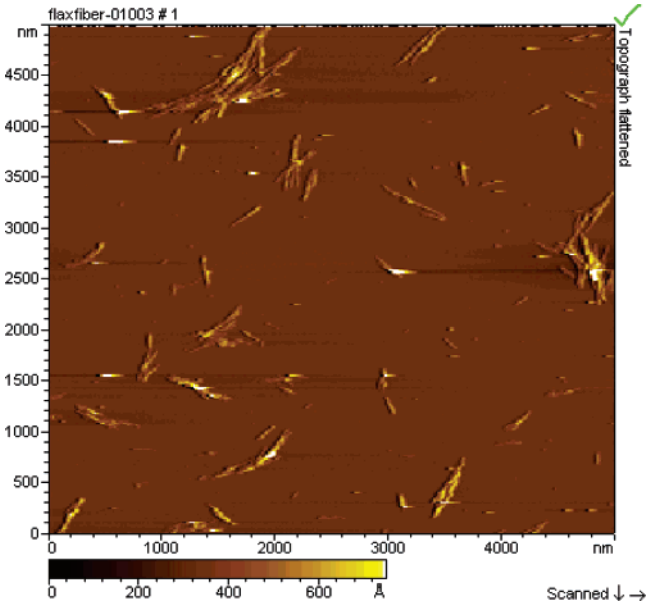

Figure 1. AFM topography image of flax cellulose nanocrystals after drying on a mica surface.

AFM measurements were carried out on a PicoSPM instrument (Molecular Imaging, Tempe, AZ) with an AFMM scanner operating in MAC mode. A type I MACLever cantilever (Molecular Imaging, Tempe, AZ) was used for MAC mode imaging. Its specifications include a force constant of approximately 0.45−5.0 N/m, and a resonant frequency of approximately 95−230 kHz. All measurements were taken with the ratio of the set-point oscillation amplitude to free air oscillation amplitude of 0.80. In addition, all measurements were performed at ambient conditions with the instrument mounted in a vibration isolation system. The scan rate was 0.5−1 lines/s (512 pixels per line) for all images. In the sample preparation, a droplet of dilute FCNs suspension was coated on a flake of mica, and the water was evaporated at ambient temperature.

Morphology of the nanocomposite films was observed with a scanning electron microscope (SEM) (S-570, Hitachi, Japan) at 20 kV. The specimens were frozen in liquid nitrogen, fractured, and then coated with gold.

Differential scanning calorimetry (DSC) measurement of the films was carried out on a DSC200 PC apparatus (Netzsch Co., Germany) under a nitrogen atmosphere. Each sample was subjected to the heating/cooling cycle between −80 and 100 °C to obtain reproducible glass transition temperature (T_g) values. The heating rate was 10 °C/min. Wide-angle X-ray diffraction patterns were recorded via X-ray diffraction (XRD-6000, Shimadzu, Japan), using Cu Kα radiation (λ = 0.154 nm) at 40 kV and 30 mA with a scan rate of 4°/min. The diffraction angle ranged from 4° to 40°.

The mechanical properties of the films were measured on a universal testing machine (CMT 6503, Shenzhen SANS Test Machine Co. Ltd., China) at room temperature with a gauge length of 5 cm and crosshead speed of 10 mm min^{-1}. An average value of at least five replicates for each sample was taken.

Results and Discussion

Morphology of FCNs and WPU/FCNs Nanocomposites. The AFM image of a dilute suspension of FCNs in Figure 1 shows that the suspension contains flax cellulose fragments consisting of both individual and aggregated nanocrystals. These fragments display slender rods and have a broad distribution in size. They have lengths (L) ranging from 100 to 500 nm and

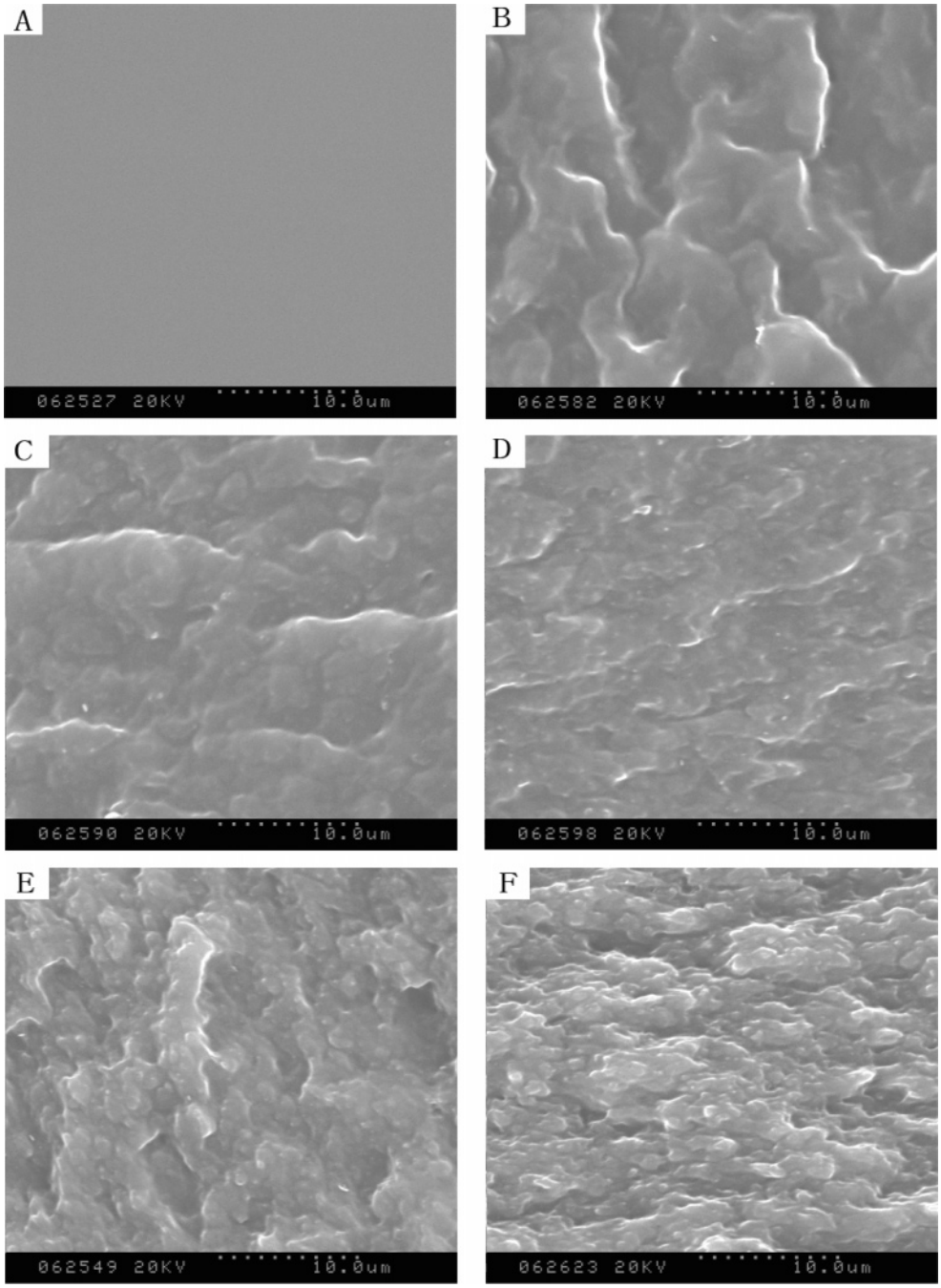

Figure 2. SEM images of the WPU/FCNs nanocoposites with different FCNs content: (A) 0 wt %; (B) 10 wt %; (C) 15 wt %; (D) 20 wt %; (E) 25 wt %; (F) 30 wt % (scale bar: 10.0 μm).

widths (*D*) ranging from 10 to 30 nm. The exact determination of the width of the nanocrystals is very difficult because of the possibility of convolution between the tip and the nanoparticle. Therefore, it is assumed that the FCNs are cylindrical, and their width is estimated from the height difference between mica surface and the nanocrystals.[49] The average length and width were estimated to be 327 ± 108 and 21 ± 7 nm, respectively. Therefore, the average aspect ratio (*L*/*D*) of the FCNs was around 15.5.

An examination of the fractured surfaces at liquid nitrogen temperature of WPU/FCNs nanocomposites was carried out using SEM. Figure 2 shows the images of WPU matrix and nanocomposites filled with 10, 15, 20, 25, and 30 wt % FCNs, respectively. As compared to the WPU film, the morphology of the FCNs can be easily identified. The FCNs appear as white dots, whose concentration on the fracture surface of the nanocomposites is increased with an increase of the filler loading. These white dots could correspond to the nanocrystals in the perpendicular plane of the nanocomposite films.[22] No large aggregates and a homogeneous distribution of the FCNs in the WPU matrix were observed in all nanocomposites, implying good adhesion between fillers and matrix. This should be attributed to the hydrophilicity of both WPU and FCNs and the hydrogen-bonding interactions existing in filler/filler and filler/matrix. Such an even and uniform distribution of the fillers in the matrix could play an important role in improving the mechanical performance of the resulting nanocomposite films as discussed later.

Structure of WPU/FCNs Nanocomposites. It is well known that the infrared spectrometer is a powerful instrument for the investigation of the hydrogen bonding behavior in polyurethane.[50] The typical polyurethane is extensively hydrogen

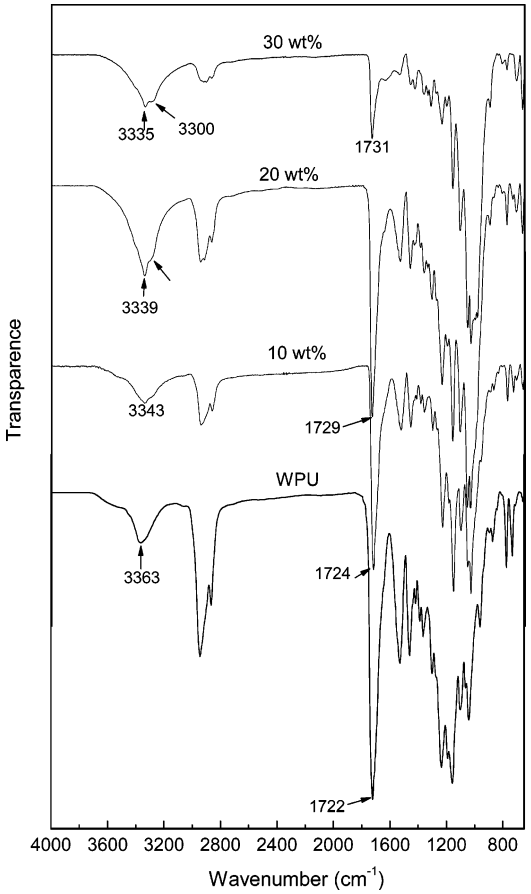

Figure 3. ATR-FTIR spectra of WPU and WPU/FCNs nanocomposites. The FCNs contents are indicated in the figure.

bonded, the donor being the NH group of the urethane linkage. Moreover, the hydrogen-bond acceptor may be in the hard segment (the carbonyl group of the urethane group) or the soft segment (ester carbonyl or ether oxygen).[51] ATR-FTIR spectra of the WPU and WPU/FCNs nanocomposites are shown in Figure 3. For WPU film, the NH stretching vibration exhibits a strong absorption peak centered at around 3363 cm^{-1} arising from the hydrogen bonding between NH and carbonyl groups, which increased the cohesion between the hard and soft segments; otherwise the free NH stretching vibration should appear at around 3420 cm^{-1}. Simultaneously, only a single prominent peak band centered at 1722 cm^{-1} assigned to the stretching vibration of both urethane and ester carbonyl was observed. This confirms the existence of the phase mixing between hard and soft segments in the WPU matrix further. With an increase of the content of FCNs in the WPU matrix, however, the peak of the carbonyl stretching vibration shifts from 1722 to 1731 cm^{-1} gradually. The shift to a higher wavenumber suggests that the incorporation of FCNs disturbs the hydrogen bonding between NH and C═O and improves the microphase separation between hard and soft segments due to the strong interaction between cellulose nanocrystal and WPU molecules. As compared to the band area of C═O, the band area located from 3200 to 3500 cm^{-1} increases with increasing FCNs content, and a shoulder peak appears at around 3300 cm^{-1}. This is attributable to the OH stretching vibration of the cellulose nanocrystals.

The WAXD of the nanocomposites was studied as a function of the FCNs content, and the corresponding diffractograms are shown in Figure 4. PCL is a kind of semicrystalline thermoplastic polymer with characteristic peaks at $2\theta = 21.5°$, 22°, and 23.5°.[52] For pure WPU, however, there is only a broad

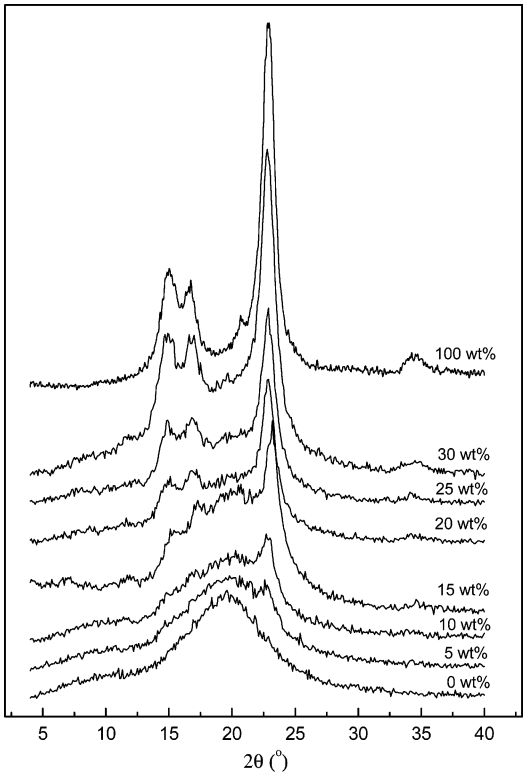

Figure 4. WAXD patterns of the WPU/FCNs nanocomposites. The FCNs contents are indicated in the figure.

diffraction hump at $2\theta = 19°$ (2θ) observed, indicating the amorphous nature of the film. It can be explained by the fact that the polyurethane prepared with PCL as soft-segments, when the M_n of PCL diol is lower than a value of around 2000, usually shows no crystallinity because the PCL molecular chain length is not long enough for chain folding.[53,54] With an addition of FCNs in the WPU matrix, some diffraction peaks appear in the diffractograms. As the FCNs content in the films increases, the peaks become more significant. When it increases up to 20 wt %, three well-defined peaks at $2\theta = 14.7°$, 16.5°, and 22.7° are observed. These diffraction peaks are present in the 100 wt % FCNs pattern at the same angles also. Therefore, it can be concluded that these diffraction peaks in the nanocomposite materials are attributable to the FCNs component. Meanwhile, no evidence of any additional peak or peak shift in the diffraction angles is observed, indicating that the diffractograms of nanocomposites are only superimpositions of the diffractograms of the two components, and the amorphous nature of WPU and the crystal structure of FCNs are unchanged.

Thermal Analysis. To further understand the structure and interaction between the two components, DSC studies of the unfilled and filled nanocomposites were performed. Figure 5 shows the DSC thermograms of WPU matrix and nanocomposites reinforced with different content of FCNs. In all of the curves, a specific heat increment is observed at around −50 °C, which corresponds to the glass−rubber transition of the soft segments of the WPU matrix, and the onset temperature is taken as the glass transition temperature (T_g). The values of T_g and the heating capacity change (ΔC_p) are shown in Table 1. In composites, the presence of FCNs can influence the values of T_g in two opposite ways. First, the solid surface of cellulose nanocrystals can induce a restricted mobility of WPU chains by forming hydrogen bonds in the interfacial area. It could result in a shift of T_g toward higher temperature. In an opposite way, the incorporation of FCNs might interrupt the original interactions between soft and hard segments and improve the mi-

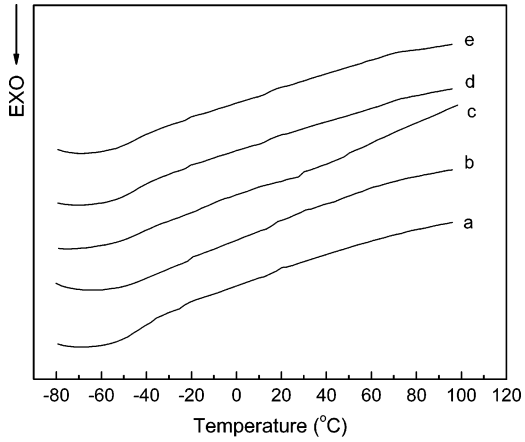

Figure 5. DSC thermograms of WPU and WPU/FCNs nanocomposites with different FCNs content: (a) 0 wt %; (b) 10 wt %; (c) 20 wt %; (d) 25 wt %; (e) 30 wt %.

Table 1. DSC Data of WPU and the WPU/FCNs Nanocomposites

sample	$T_{g,onset}$ (°C)	ΔC_p (J g^{-1} K^{-1})	sample	$T_{g,onset}$ (°C)	ΔC_p (J g^{-1} K^{-1})
WPU	−51.4	0.36	WPU/FCNs-20	−53.8	0.24
WPU/FCNs-5	−52.3	0.32	WPU/FCNs-25	−53.7	0.26
WPU/FCNs-10	−52.9	0.33	WPU/FCNs-30	−54.1	0.20
WPU/FCNs-15	−53.1	0.35			

crophase separation in WPU. This effect can result in a decrease of T_g of soft segment indirectly. However, the interactions between two kinds of polymers are far less than the chemical linkages between the soft and hard segments, which can be proved by a decrease in the values of T_g and ΔC_p for the WPU/FCNs nanocomposites, as compared to WPU.[55] Therefore, the downward trend of T_g of the nanocomposites in our work could be attributed to the improvement of the degree of freedom for the soft segment in WPU, as a result of an improvement of microphase separation between soft and hard segments. In addition, no endothermic peaks, assigned to the melting of PCL (soft segment) crystalline, are observed in all curves, indicating the amorphous nature of the WPU matrix. This is in good agreement with the result from WAXD.

Mechanical Properties. The mechanical behavior of the films of neat WPU matrix as well as the nanocomposites reinforced with various contents of FCNs was investigated by tensile testing at room temperature. Figure 6 shows the stress−strain curves of the seven film materials. Clearly, two characteristic regions of deformation behavior can be observed. At low strains (<10%), the stress increases rapidly with an increase in strain, and the Young's modulus was measured from the initial slopes in the elastic region. At higher strain, the stress regularly increases with the strain increasing up to the break of the films. No evidence of necking phenomenon at the stress−strain curves confirms the good dispersion of the FCNs in the matrix and homogeneous morphology of the nanocomposites.

The Young's modulus, tensile strength, and elongation at break were determined from the curves, and the results are presented in Table 2. Because of its amorphous nature, the WPU displays a nonlinear elastic behavior and possesses a low tensile strength of 4.27 MPa and a low tensile modulus of 0.50 MPa as well as a high elongation at break of about 1086%. From Table 2, we can see that the FCNs content has a profound effect on the tensile properties. The tensile strength increases significantly from 4.3 to 14.9 MPa with increasing filler content from 0 to 30 wt %, whereas the elongation at break decreases from 1086% to 186%. This indicated that incorporating FCNs into the WPU matrix resulted in strong interactions between fillers

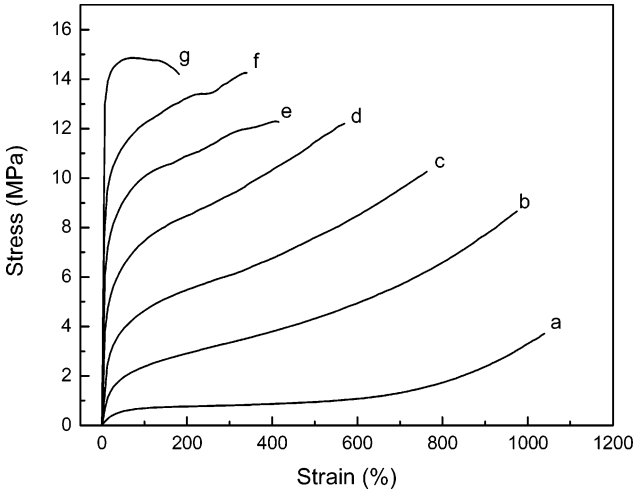

Figure 6. Stress−strain curves of WPU/FCNs nanocomposite films with FCNs content: (a) 0 wt %; (b) 5 wt %; (c) 10 wt %; (d) 15 wt %; (e) 20 wt %, (f) 25 wt %; (g) 30 wt %.

Table 2. Mechanical Properties of WPU and the WPU/FCNs Nanocomposites Obtained from Tensile Tests: Young's Modulus (E), Tensile Strength (σ_B), and Elongation at Break (ϵ_B)

sample	E (MPa)	σ_B (MPa)	ϵ_B (%)
WPU	0.5 ± 0.1	4.3 ± 0.8	1086.4 ± 30.3
WPU/FCNs-5	0.7 ± 0.3	9.3 ± 1.3	986.6 ± 36.9
WPU/FCNs-10	7.8 ± 0.2	10.2 ± 1.9	735.5 ± 32.3
WPU/FCNs-15	47.5 ± 1.8	12.1 ± 1.8	614.9 ± 20.6
WPU/FCNs-20	116.6 ± 6.7	12.3 ± 2.0	420.8 ± 25.6
WPU/FCNs-25	236.9 ± 12.5	14.2 ± 1.4	340.1 ± 18.7
WPU/FCNs-30	334.4 ± 10.9	14.9 ± 1.2	186.1 ± 20.1

and between filler and matrix, which restricted the motion of the matrix. It is worth noting that the Young's modulus increases nearly exponentially with FCNs content, from 0.5 MPa for the pure WPU to about 344 MPa for the film WPU/FCNs-30. Especially, the WPU/FCNs-10 has a value about 10 times higher than that of WPU/FCNs-5, which is very near to that of pure WPU. This phenomenon can be explained by the fact that the rigid filler network, which could be responsible for the unusual enforcing effect, has been formed as the FCNs content is higher than 10 wt % in the matrix. As reported by Favier et al., for a three-dimensional network, the volume fraction of the cellulose nanocrystals was required to reach a percolation threshold (V_{Rc}), which depends on the aspect ratio of the cellulose nanocrystals and can be estimated by $V_{Rc} = 0.7/(L/D)$.[22] With substitution of the L/D value of 15.5 for FCNs into above equation, V_{Rc} = 4.5 vol %, 6.7 wt % can be obtained, taking 1.5 and 1.08 g cm^{-3} for the density of crystalline cellulose and the WPU matrix, respectively.[50−56]

Conclusions

A suspension of cellulose nanocrystals, with an average length of 327 ± 108 nm and a diameter of 21 ± 7 nm, was prepared from flax fibers by acid hydrolysis and used to reinforce the WPU matrix with content from 5 to 30 wt % for the preparation of nanocomposite materials by the casting method. The results from ATR-FTIR and SEM indicated that the FCNs fillers were well dispersed within the WPU matrix and had good adhesion in the interfacial area due to the strong hydrogen bonding. Meanwhile, the incorporation of FCNs resulted in an improvement of microphase separation between soft and hard segments

in WPU, leading to a decrease of T_g and ΔC_p for the nanocomposite films. It is worth noting that the FCNs-filled nanocomposites show an increase in Young's modulus and tensile strength from 0.5 to 344 MPa and 4.3 to 14.9 MPa, respectively, with an increase of the fillers content from 0 to 30 wt %. This is mainly due to the three-dimension networks of intermolecular hydrogen-bonding interactions between filler and filler and between filler and matrix. The superior properties of the new nanocomposite materials could have great potential applications.

References and Notes

(1) Li, S.; Vatanparast, R.; Lemmetyinen, H. *Polymer* **2000**, *41*, 5571−5576.
(2) Modesti, M.; Lorenzetti, A. *Eur. Polym. J.* **2001**, *37*, 949−954.
(3) Kim, C. K.; Kim, B. K. *J. Appl. Polym. Sci.* **1991**, *43*, 2295−2301.
(4) Chan, W. C.; Chen, S. A. *Polymer* **1993**, *34*, 1265−1270.
(5) Dreja, M.; Heine, B.; Tieke, B.; Junkers, G. *J. Colloid Interface Sci.* **1997**, *191*, 131−140.
(6) Wicks, Z. W.; Wicks, D. A.; Rosthauser, J. W. *Prog. Org. Coat.* **2002**, *44*, 161−183.
(7) Busato, F. *Macromol. Symp.* **2002**, *187*, 17−21.
(8) Kuan, H.; Ma, M.; Chang, W.; Yuen, S.; Wu, H.; Lee, T. *Compos. Sci. Technol.* **2005**, *65*, 1703−1710.
(9) Hsu, S.; Tang, C.; Tseng, H. *J. Biomed. Mater. Res., Part A* **2006**, *79A*, 759−770.
(10) Kim, B.; Seo, J.; Jeong, H. *Eur. Polym. J.* **2003**, *39*, 85−91.
(11) Lee, H.; Lin, L. *Macromolecules* **2006**, *39*, 6133−6141.
(12) Lee, H.; Hwang, J.; Liu, H. *J. Polym. Sci., Part A: Polym. Chem.* **2006**, *44*, 5801−5807.
(13) Kuan, H.; Ma, C.; Chuang, W.; Su, H. *J. Polym. Sci., Part B: Polym. Phys.* **2005**, *43*, 1−12.
(14) Kwon, J.; Kim, H. *J. Polym. Sci., Part A: Polym. Chem.* **2005**, *43*, 3973−3985.
(15) Kwon, J.; Kim, H. *J. Appl. Polym. Sci.* **2005**, *96*, 595−604.
(16) Kuan, H.; Ma, C.; Chang, W.; Yuen, S.; Wu, H.; Lee, T. *Compos. Sci. Technol.* **2005**, *65*, 1703−1710.
(17) Hsu, S.; Chou, C.; Tseng, S. *Macromol. Mater. Eng.* **2004**, *289*, 1096−1101.
(18) Sturcova, A.; Davies, G. R.; Eichhorn, S. J. *Biomacromolecules* **2005**, *6*, 1055−1061.
(19) Helbert, W.; Cavaille, J. Y.; Dufresne, A. *Polym. Compos.* **1996**, *17*, 604−611.
(20) Podsiadlo, P.; Choi, S.; Shim, B.; Lee, J.; Cussihy, M.; Kotov, N. *Biomacromolecules* **2005**, *6*, 2914−2918.
(21) Azizi Samir, M. A. S.; Alloin, F.; Dufresne, A. *Biomacromolecules* **2005**, *6*, 612−626.
(22) Favier, F.; Chanzy, H.; Cavaille, J. Y. *Macromolecules* **1995**, *28*, 6365−6367.
(23) Fengel, D.; Wegner, G. *Wood: Chemistry, Ultrastructure, Reactions*; Walter de Gruyter: New York, 1984.
(24) Mathew, A. P.; Dufresne, A. *Biomacromolecules* **2002**, *3*, 609−617.
(25) Terech, P.; Chazeau, L.; Cavaille, J. Y. *Macromolecules* **1999**, *32*, 1872−1875.
(26) Revol, J. F. *Carbohydr. Polym.* **1982**, *2*, 123−134.
(27) Hanley, S. J.; Giasson, J.; Revol, J. F.; Gray, D. G. *Polymer* **1992**, *33*, 4639−4642.
(28) Tokoh, C.; Takabe, K.; Fujita, M.; Saiki, H. *Cellulose* **1998**, *5*, 249−261.
(29) Grunert, M.; Winter, W. T. *J. Polym. Environ.* **2002**, *10*, 27−30.
(30) Lu, Y.; Weng, L.; Cao, X. *Carbohydr. Polym.* **2006**, *63*, 198−204.
(31) Araki, J.; Wada, M.; Kuga, S.; Okano, T. *Colloids Surf., A* **1998**, *142*, 75−82.
(32) Beck-Candanedo, S.; Roman, M.; Gray, D. G. *Biomacromolecules* **2005**, *6*, 1048−1054.
(33) Dubief, D.; Samain, E.; Dufresne, A. *Macromolecules* **1999**, *32*, 5765−5771.
(34) Dufresne, A.; Kellerhals, M. B.; Witholt, B. *Macromolecules* **1999**, *32*, 7396−7401.
(35) Dufresne, A. *Compos. Interfaces* **2003**, *10*, 369−388.
(36) Angles, M. N.; Dufresne, A. *Macromolecules* **2000**, *33*, 8344−8353.
(37) Angles, M. N.; Dufresne, A. *Macromolecules* **2001**, *34*, 2921−2931.
(38) Noshiki, Y.; Nishiyama, Y.; Wada, M.; Kuga, S.; Magoshi, J. *J. Appl. Polym. Sci.* **2002**, *86*, 3425−3429.
(39) Helbert, W.; Cavaille, J. Y.; Dufresne, A. *Polym. Compos.* **1996**, *17*, 604−611.
(40) Chazeau, L.; Cavaille, J. Y.; Canova, G.; Dendievel, R.; Boutherin, B. *J. Appl. Polym. Sci.* **1999**, *71*, 1797−1808.
(41) Ljungberg, N.; Bonini, C.; Bortolussi, F.; Boisson, C.; Heux, L.; Cavaille, J. Y. *Macromolecules* **2005**, *6*, 2732−2739.
(42) Matos Ruiz, M.; Cavaille, J. Y.; Dufresne, A.; Graillat, C.; Gerard, J. F. *Macromol. Symp.* **2001**, *169*, 211−222.
(43) Matos Ruiz, M.; Cavaille, J. Y.; Dufresne, A.; Gerard, J. F.; Graillat, C. *Compos. Interfaces* **2000**, *7*, 117−131.
(44) Cavaille, J. Y.; Dufresne, A.; Paillet, M.; Azizi Samir, M. A. S.; Alloin, F.; Sanchez, J. Y. French Patent FR2841255.
(45) Bos, H. L.; van den Oever, M. J. A.; Peters, O. C. J. J. *J. Mater. Sci.* **2002**, *37*, 1683−1692.
(46) Smeder, B.; Liljedahl, S. *Ind. Crop. Prod.* **1996**, *5*, 149−162.
(47) Dong, X. M.; Kimura, T.; Revol, J. F.; Gray, D. G. *Langmuir* **1996**, *12*, 2076−2082.
(48) Marchessault, R. H.; Morehead, F. F.; Walter, N. M. *Nature* **1959**, *184*, 632−633.
(49) Kvien, I.; Tanem, B. S.; Oksman, K. *Biomacromolecules* **2005**, *6*, 3160−3165.
(50) Cao, X.; Zhang, L. *Biomacromolecules* **2005**, *6*, 671−677.
(51) Seymour, R. W.; Cooper, S. L. *Macromolecules* **1973**, *6*, 48−53.
(52) Sarasam, A. R.; Krishnaswamy, R. K.; Madihally, V. *Biomacromolecules* **2006**, *7*, 1131−1138.
(53) Heijkants, R. G. J. C.; van Calck, R. V.; van Tienen, T. G.; de Groot, J. H.; Buma, P.; Pennings, A. J.; Veth, R. P. H.; Schouten, A. J. *Biomaterials* **2005**, *26*, 4219−4228.
(54) Ping, P.; Wang, W.; Chen, X.; Jing, X. *Biomacromolecules* **2005**, *6*, 587−592.
(55) Gao, S.; Zhang, L. *Macromolecules* **2001**, *34*, 2202−2207.
(56) Azizi Samir, M. A. S.; Alloin, F.; Sanchez, J. Y.; Kissi, N. A.; Dufresne, A. *Macromolecules* **2004**, *37*, 1386−1393.

BM0610368